Climate aridity delays morphological response of Andean river valleys to tectonic uplift

Climate aridity delays morphological response of Andean river valleys to tectonic uplift

Rebekah Harries*[1,2], Felipe Aron [1,2, 3] and Linda A. Kirstein [4]

[1] Departamento de Ingeniería Estructural y Geotécnica, Escuela de Ingeniería, Pontificia Universidad Católica de Chile, Campus San Joaquín, Av. Vicuña Mackenna 4860, Macul, Santiago, Chile

[2] Research Center for Integrated Disaster Risk Management (CIGIDEN), Edificio Hern´an Briones, Campus San Joaquín, Pontificia Universidad Cat´olica de Chile, Av.

[3] Now at Departamento de Geología, Universidad de Chile, Plaza Ercilla 803, Santiago, Chile

[4] School of Geosciences, Grant Institute, University of Edinburgh, Edinburgh, UK, EH9 3FE

*Corresponding author:

Present address: Institute of Hazard, Risk and Resilience, Durham University Lower Mount Joy, South Rd, Durham DH1 3LE

Email: rebekah.m.harries@durham.ac.uk

Abstract

In the South Central Andes, a complex relationship between climate, tectonics, erosion and topography is well documented. Building on recent advances in the mechanical modelling of subduction zones, we isolate the contribution of fault motion to topography and observe how rock uplift has been recorded in river valley morphology. Rivers on the wetter Chilean-side of the Andean cordillera have steep and narrow valleys, in stark contrast to those draining the arid Argentinian cordillera, whose valleys are variably wider and less steep. The Chilean rivers have responded to fault slip along the western mountain front by incising vertically and propagating a knick zone upstream. In Argentina, there is little evidence of channel steepening despite predictions for higher vertical rock uplift rates. We hypothesise that the aridity of the Argentinian region has limited the transport capacity of the rivers to export their sediment fill and as a result, vertical incision has been inhibited and lateral incision and valley widening favoured. The long-term climate gradient appears to have been important in modulating the morphological response of these rivers to fault slip. These factors precondition future landscape sensitivity to both tectonic and climatic change.

Keywords: Climate, tectonics, river, sediment, Andes, subduction zone

1. Introduction

The relationship between rock uplift and river incision underpins our understanding of how, and at what pace, landscapes evolve and respond to tectonic and climatic change (Adams et al., 2020). As the climate shifts, there is now a need to identify erosion and sedimentation hotspots in landscapes and assess their future potential for generating geomorphic hazards cascades that propagate downstream (Schwanghart et al., 2018; Barnhart et al., 2020). The complex feedbacks between climate, sediment transport, erosion, and topography, however, are not well understood, nor easily isolated from tectonics. If we are to deduce the impact of climate on spatially and temporally varying erosion trends, the contribution of rock uplift to topography needs to be well constrained by integrating field and modelling approaches. In this paper, we explored to what extent the geomorphological evolution of a river's sediment routing system modulates a river's incisional response to rock uplift, when uplift is driven by plate subduction. More specifically, we assessed whether steeper topography, and higher millennial and decadal erosion rates, along the south-Central Andean subduction zone, between 33 and 37◦S, is the result of higher rock uplift rates or whether they record a more complex relationship with erosion and climate. In doing so, we bridge the gap between shallow surface and deep Earth processes to understand the evolution of topography.

Observations of the link between erosion and uplift are centred around the ubiquitous power law relationship between channel slope and drainage area that is measurable in real landscapes. Many field studies have focused on modelling this observation with stream power geomorphic incision rules in tectonically active landscapes (e.g. Goren et al., 2014; Kirby and Whipple, 2001; Leonard and Whipple, 2021; Racano et al., 2021; Aron et al., 2022). This detachment-limited style model implicitly assumes river profiles evolve to maintain a transport capacity equal to its sediment flux, such that the bed resistance to detachment by the flow controls the incision rate. This means that bedrock rivers erode at a rate equivalent to their uplift rate, relative to base level, and remove all the sediment they are supplied with. In this way, channel steepness (the steepness of a channel normalised by its drainage area) is considered an indicator of the vertical incision rate and dependent on the tectonic and climatic boundary conditions acting on the landscape (Kirby and Whipple, 2012; Hilley et al., 2019). Where channel steepness can be normalised by a uniform value of profile concavity, spatial patterns in steepness are being increasingly used to map spatial variability in tectonic uplift or bedrock erodibility (Kirby and Whipple, 2001; Goren et al., 2014; Leonard and Whipple, 2021; Racano et al., 2021; Aron et al., 2022), assuming erosion has kept pace with uplift and is time-invariant (Perron and Royden, 2013). This assumption that erosion has kept pace with uplift, however, is limiting in many settings and is particularly restrictive when exploring the impact of climate on river channel networks.

As rock uplift increases the height of mountain ranges, mass wasting increases the delivery of sediment to river valleys. Rivers are tasked with evacuating and redistributing this sediment in order to incise. Numerous models that incorporate sediment transport thresholds and sediment flux dependencies in bedrock river evolution, highlight the role of a river's sediment transport capacity in modulating its

incisional response to uplift. Models suggest that both the spatial distribution of rock uplift and the distribution of sediment across a river network control the morphology of fluvial landscapes (Gasparini and Brandon, 2011). Mechanistic models demonstrate that for a given uniform tectonic uplift field, river incision rates can vary over several orders of magnitude, depending on the degree of coupling between the supply of sediment to a river and the river's sediment transport capacity (Sklar and Dietrich, 2006). Similarly, when bedrock erosion is increasingly dependent on sediment transport, equilibrium channel slopes and relief within mountain ranges are found to be lower than would be expected for detachment-limited models of river incision (Whipple, 2002). This is because, as rivers become predominantly alluvial, channel gradient becomes more dependent on sediment and water fluxes to the channel and their interaction with the bed, rather than any tectonically induced slope (Wickert and Schildgen, 2019). In which case, the degree to which a mountain river's bed is covered with sediment modulates whether it is protected by an alluvial cover or exposed to sediment tools for erosion (Sklar and Dietrich, 2004; Yanites et al., 2011).

Beyond models, field studies demonstrate that the link between tectonics, climate and river profile form is also modulated by adjustments in channel width, sediment size and lithology (Riebe et al., 2015; Yanites, 2018; Harries et al., 2018; Baynes et al., 2020; Shobe et al., 2021). The preference for rivers to erode laterally as well as vertically has been linked to rock uplift and sediment supply as well as the hardness of the transported sediment (Brocard and van der Beek, 2006). Alluvial covers are found to inhibit both vertical and lateral incision rates in the field (Cook et al., 2014), while models suggest that the frequency of bed impacts by sediment particles as well as the volume of sediment detached from the bed by each impact, influences lateral erosion rates (Li et al., 2020).

The supply of sediment downstream is therefore a key modulator of bedrock incision. The supply, however, is not only dependent on the processes of sediment generation, i.e. faulting, chemical and physical weathering (Riebe et al., 2015). It is also dependant on factors that control sediment transfer. These are the degree of connectivity between sediment sources and active channels (Harries et al., 2021) and the capacity of the rivers to transport sediment along them (Shobe et al., 2021; Lai et al., 2021). Climate drives cascades of geomorphic adjustments that modulate the availability and mobility of sediment within the landscape (Harrison et al., 2019; Wapenhans et al., 2021). Climate should therefore be a key control on the distribution of sediment in the landscape and, in turn, influence the dependency of bedrock erosion on sediment transport and the resultant spatial variability in bedrock erosion (Hobley et al., 2011).

This complicates a direct relation between climate, bedrock incision and topographic form that is predicted by the detachment-limited stream power incision model. Indeed, where it is expected that a higher mean annual precipitation rate will generate more stream power and enhance incision (e.g. Ferrier et al., 2013), the impact of climate on river channel steepness is in fact not persistently detected in real landscapes (Leonard and Whipple, 2021; Desormeaux et al., 2022). The geomorphological evolution of a river's sediment routing system should be a critical filter for climate driving bedrock erosion. The lack of constraint on the geomorphological evolution of river valleys limits our understanding of how vulnerable they are to shifts in climate over the next century.

It also limits our understanding of how sediment storage and evacuation might modulate bedrock incision and valley evolution (Lague, 2010). Extreme rainfall events can evacuate sediment generated by earthquake triggered landslides rapidly (Dadson et al., 2004), while glacial-interglacial cycles can influence sediment storage and transfer over much longer periods (Dosseto et al., 2010).

For this investigation we selected the south-Central Chilean-Argentinian Andes, a region characterised by strong tectonic and climatic gradients that have been repeatedly explored as drivers of latitudinal variability in mountain topography and erosion rates (e.g. Carretier et al., 2018; Val et al., 2018; Montgomery et al., 2001; Lamb and Davis, 2003; Stalder et al., 2020; Seagren et al., 2020; Evenstar et al., 2023).

Latitudinally, differences between decadal, millennial, and longer-term erosion patterns, and how they relate with topography, have indicated varying degrees of landscape transience in response to rock uplift (Carretier et al., 2018). The lack of reliable, quantitative methods for measuring pure tectonic uplift (England and Molnar, 1990; Hoggard et al., 2021), and our short time window of observation, however, are the primary limitations to deconvolving the tectonic and climatic influences on erosion and topography (Perron, 2017).

To address part of those limitations, we exploited recent advances in the modelling of subduction zones to predict differential rock uplift caused by crustal-scale faults and thereby isolate the contribution of tectonic uplift to mountain relief. This method is powerful because it allows us to map spatially the variability in tectonic uplift driven by subduction zone mechanics. We can therefore explore the relative importance of climate, bedrock lithology and glaciation on spatial variability in mountain river morphology. We investigated how the steepness and width of mountain rivers, and their local topography, have recorded the predicted fault activity. We use these observations to highlight areas of the mountain range that may be susceptible to change as the climate shifts.

2. Study area

The Andes between 33 and 37◦S are an evolving tectonic-volcanic landscape with strong spatial gradients in climate and glaciation (Fig. 1). While several of the highest peaks in this region are volcanoes, deformed rock also outcrops at >5000 m. The topography of the mountain range is a major topographic barrier to moisture delivered by westerlies and has influenced the mean annual precipitation, seasonality and storminess of the climate both sides of the drainage divide, persistently over at least the last 14 Myr (Rehak et al., 2010; Viale et al., 2019). On both the western, Chilean Andes and eastern, Argentinian Andes, Ushaped valleys and large ridges of glacial moraine in the upper reaches of catchments are evidence to suggest glaciers have been important in shaping their upper reaches through the Quaternary (Farías et al., 2008). Downstream, mountain rivers are bedrock-alluvial channels, which in Chile encompass large terrace sequences (Fig. 2). The history and timescales of sediment storage and evacuation that are evident in undated and unmapped valley fills and fluvial terrace sequences, however, is unknown. The geomorphological evolution of

the south Central Andes has been left poorly constrained, in contrast to its structural history.

The most recent episode of horizontal shortening and crustal thickening began during the Miocene (~25 Ma) when convergence rates between the South American and Nazca plates may have increased (e.g. Litvak et al., 2018). Since then, plate motion has been accommodated through contraction and uplift of the Principle and Frontal Cordilleras on a mixture of steep structures rooted in basement and flat and ramp thrusts across the sedimentary cover (e.g., McQuarrie and DeCelles, 2001; McQuarrie, 2002; Müller et al., 2002; Pearson et al., 2013; Giambiagi et al., 2003; Riesner et al., 2018). The onset, intensity, and localisation of deformation along these structures, and their relative importance in accommodating uplift, vary with latitude. This alongstrike variability has been linked to both changes in subduction geometry (Kay and Mpodozis, 2002) and climatically forced variability in erosion (Montgomery et al., 2001). A southward reduction in mountain elevation across the study area has been previously linked to climate. The reduction in peak height being driven either by a southward increase in glacial erosion, evident from decreasing snow line altitudes southwards (Montgomery et al., 2001), or, in parallel, due to a southward increase in the volume of sediment delivered to the Chilean Trench, which can reduce the friction at the plate boundary and dampen crustal deformation (Lamb and Davis, 2003).

In contrast to these denudation patterns on geological timescales, millennial and decadal erosion rates calculated from cosmogenic nuclides and suspended sediment yields peak around 33◦S, and therefore record a more recent decreasing erosion trend southward, within the western Chilean Cordillera, which goes against the precipitation gradient (Carretier et al., 2015). This erosion peak at 33◦S coincides with the highest topography, with peaks over 6000 m, though not with mean hillslope gradient (Rehak et al., 2010). Carretier et al. (2015) proposed that the difference between millennial and longer-term erosion patterns may be explained by the landscapes reflecting different stages in their transient topographic response to uplift, modulated by climate. In the arid north, they suggest similar long-term and millennial erosion rates and the occurrence of relict perched pediments (Rehak et al., 2010) is evidence of a very long and slow erosive response to uplift. In the wet south, the topographic response to uplift may have been accelerated, particularly through glacial erosion (Melnick and Echtler, 2006) and has had its erosional peak pass millions of years ago, first filling the subduction trench with sediment, and then leaving behind a landscape with decreasing slopes and low erosion rates. Where erosion peaks around 33oS, in the central Chile, Carretier et al. (2015) suggest river knickpoints are propagating upstream and reaching the catchment head (e.g., Farías et al., 2008) and are therefore closest to being in equilibrium with uplift. Below, the tectonic, lithologic and climatic evolution of Chilean-Argentinian Andes within our targeted study site, between 33 and 37◦S, is detailed.

2.1. Tectonic landscape

Four major crustal-scale structures accommodate shortening in this region: (i) San Ramon-Pocuro; (ii) El Diablo-Las Leˇnas-El Fierro; (iii) Malargüe-Aconcagua fold and thrust belt; and (iv) Frontal Cordillera (Fig. 1a) (Farías et al., 2010). The partitioning of

deformation across these four crustal-scale structures (Fig. 1a), however, is highly contested (Armijo et al., 2010; Farías et al., 2010; Giambiagi et al., 2003; Vargas et al., 2014; Riesner et al., 2018), though linked to local variability in subduction geometry and convergence rate (Arriagada et al., 2013).

It is generally accepted that the Andes between 33 and 37◦S uplifted relatively simultaneously since the late Miocene (Carretier et al., 2015 and references therein). From ~25 Ma, crustal thickening and shortening drove folding and thrusting within Mesozoic beds, now on the Argentinian-side of the cordillera, and deformed the late Eocene-Oligocene volcanic beds of the Abanico and Farellones formations, which now outcrop on the Chilean-side of the cordillera (Farías et al., 2010). Initial uplift of the Argentinian-side, along the Aconcagua and Malargüe fold-and-thrust belts, occurred between ~25 and 10 Ma, with deformation propagating eastwards from 13 Ma. After 9 Ma, the El Diablo-Las Lenas-El Fierro fault system, which bounds the Abanico and Farellones formations and approximates the location of the drainage divide, was activated. This fault system is still seismically active today (Farías et al., 2010). Deformation at the front of the Malargüe fold-andthrust belt, within the Malargüe anticline began after 7 Ma and continued until 1 Ma (Silvestro et al., 2005). On the Chilean-side, deformation initially occurred between 25 and 22 Ma, within the Abanico formations (Armijo et al., 2010), with an episode of more recent, rapid uplift between 10.5 and 4.6 Ma (Farías et al., 2008). Farías et al. (2008) derived the timing of this recent event by mapping out the propagation of knickpoints, still preserved in this region's river profiles, across uplift markers and dated volcanic bodies. The celerity of knickpoint propagation they estimated to be 10–40 mm a□ 1. The uplifting fault, the San Ramon-Pocuro fault, is now believed to only be seismically active in the north of the study area (Vargas et al., 2014; Riesner et al., 2017). These four major structures were incorporated into the tectonic model.

2.2. Bedrock landscape

The drainage divide of the Principle Cordillera roughly corresponds with the El Diablo-Las Leˇnas-El Fierro fault system, which marks the approximate contact between Mesozoic and Cenozoic deposits exposed in the eastern and western sides of the cordillera, respectively (Fig. 1). On the Argentinian-side of the drainage divide, the Malargüe and Aconcagua fold-and-thrust belts expose Mesozoic interbedded marine and continental strata with small outcrops of pre-Jurassic basement quartzites and schists. Pliocene to Holocene volcanic rocks are also exposed locally, around large eruptive centres (Mescua et al., 2014). Bedrock exposed on the Chilean-side of the drainage divide, however, is predominantly made up of Cenozoic volcaniclastic rocks, tuffs, basic lavas, ignimbrites, and interbedded alluvial, fluvial, and lacustrine sediments (SERNAGEOMIN 1:1 M geo map). This sequence is capped in some areas by intermediate and basic lava strata with volcanic rocks and minor ignimbrite beds. Bedrock on the most western front is notably deformed and intruded with granitic rocks <10 Ma old (Farías et al., 2008). Tolorza et al. (2019) identified the Mesozoic rocks in this region as more resistant to slope failure, than the Cenozoic rocks. Farías et al. (2008) suggested that the localisation of knickpoints and steeper channels within this belt of granitic outcrops records the influence of spatial variability in bedrock hardness on erosion.

2.3. Climate

Latitudinal variability in precipitation patterns, vegetation (Jeffery et al., 2014) and ice cover (Rehak et al., 2010; Viale et al., 2019) are driven by the northward penetration of frontal systems associated with the westerlies, as far north as 30◦S. Between 33 and 37◦S, there is a marked transition from subtropical to extratropical climate which impacts how moisture is distributed across the cordillera. In the western Principle Cordillera, precipitation predominantly falls in the cold seasons and is often frozen, whereas in the east, precipitation is concentrated in convective summer storms (Poveda et al., 2020). While precipitation rates are comparably low on both sides of the Andes north of 35◦S (~400 mm/yr), southwards precipitation rates increase by a factor of 2 on the western slopes of the cordillera (~1500 mm/yr) (Rehak et al., 2010).

Southward increases in precipitation rates are also accompanied by a lowering of the 0 ◦C isotherm from >4000 m altitude in the north to ~3000 m in the south (Masiokas et al., 2020). Recent glacial inventories show the highest concentration of glaciers and rock glaciers in South America between 31 and 35◦S, largely due to the frequency of peaks above 5000 m (Masiokas et al., 2020). The southward reduction in mountain elevation (Fig. 1) means that, across the study area, glaciers become more sparse southwards, despite the accompanying increase in precipitation and lowering of the 0 ◦C isotherm from >4000 m altitude to ~3000 m. Across the drainage divide, glaciers on western slopes are found to descend 500 m lower than those on the east (Masiokas et al., 2020).

The rivers investigated are perennial rivers that experience strong seasonality between the winter and snowmelt seasons (Fig. 1c). In the Rio Maipo, Chile, variability in average monthly discharge is 50 %, with historical average monthly discharges during snowmelt season of 151 m^3/s and during winter, around 57 m^3/s (Arrospide et al., 2018). Whereas in Argentina, the average monthly discharge of the Rio Atuel varies by ~170 %, with 22 m^3/s and 65 m^3/s in the winter and melt seasons, respectively (Araneo and Villalba, 2014).

The differences in both mean annual precipitation and discharge variability across this region of the mountain range are ideal for probing the impact of spatially variable climate on mountain river morphology. Especially as it lies within the range of precipitation values that models suggest landscapes should be most sensitive to; mean annual precipitation between 100 mm/yr and 1500 mm/yr (DiBiase and Whipple, 2011).

3. Methods

3.1. Topographic analysis

We characterise the morphology of the seven major perpendicular rivers draining the Principle Cordillera (Fig. 3) by calculating their normalised channel steepness and local relief from a 12 m DEM and measuring their bedrock valley widths.

In calculating channel steepness, we test the assumption that the rivers on both sides of the Andean drainage divide are steepening in response to zones of enhanced tectonic uplift. This ought to be the case if the rivers are responding to uplift in a

detachment-limited way. Where rivers are not steepening, we can then identify them as being less sensitive to their tectonically induced slope and transport-limited. We calculate normalised channel steepness (ksn) using the gradient of elevation along a channel (S) and the upstream area (A), normalised it by a median concavity value (θ) of 0.37, for all seven rivers (ksn).

$ksn = S/A^{-\theta}$

The median value was identified using the TopoToolbox algorithm, which tunes the Bayesian Optimization of the parameter to all catchments in the study area through cross validation (Schwanghart and Scherler, 2014). This normalisation of channel steepness indices allows us to compare indices across the study area.

The distributions of ksn within each bedrock lithology group, for all points along the river network, were then derived and compared between river catchments to analyse the dependency of channel steepness on bedrock lithology. We exploit existing geological maps (1:1 M) published by the geological surveyors of Chile and Argentina, SERNAGEOMIN and SEGEMAR, respectively, to group bedrock lithologies using the available relevant data that we expect to influence their resistance to erosion; their age and lithology.

The local relief of the cordillera was calculated from the elevation range within a 5 km moving window using the TopoToolbox local relief algorithm (Schwanghart and Scherler, 2014). To directly observe the difference between the spatial variability in normalised channel steepness, local relief, and the predicted tectonic uplift field, we convert these data to rasters and scale their variability between 0 and 1. We then subtract the tectonic uplift field from the steepness and local relief maps.

Valley width measurements were taken every two kilometres along the main river valley (Fig. 3 inset) using Google Earth satellite imagery (0.5 m resolution) and in some localities verified with field measurements.

3.2. Tectonic model

Existing thermochronology and provenance studies between 33° and 37°S generally agree that rock uplift occurred relatively synchronously during a main exhumation event since the Late Miocene (Stalder et al., 2020). This shared uplift history allows the spatiotemporal evolution of faulting in this region to be averaged over a timescale equivalent to rates of long-term plate convergence. We create a 3D model of this segment of the Andean subduction zone and impose boundary conditions and far field loads to simulate the long-term subduction that excites slip on crustal faults.

To calculate the spatial variability in rock uplift, we built a mechanical Boundary Elements Method (BEM) model of the plate boundary (Fig. A2). For this we used the 3D BEM Matlab© code tribemx (Loveless, 2019). This code uses line integral algorithms relating slip on triangular dislocation elements to displacement and strain throughout a homogeneous elastic half-space, solving the boundary value problem based on elastic dislocation theory (Meade, 2007). Due to its elastic nature, the model does not allow plastic yielding of the material and gravity loads were set to zero. The

BEM is a natural choice for modelling faults as it requires that only dislocation surfaces be parameterised within a three dimensional body (e.g. Marshall et al., 2009).

A 3D mesh of the Andean subduction zone was first constructed by parameterising the major structures described previously as a series of dislocation surfaces embedded in the half-space, meshed with planar triangular elements using the public software Gmsh© (Geuzaine and Remacle, 2009). The model half-space was parameterised as a 650 × 300 km box, with the long axis orientated parallel to the vector of plate motion (Figs. 1 and 3) and with a maximum depth of 270 km, from the traction-free boundary at the surface of the Earth to the base of the subducting oceanic plate. The surface of the Earth was considered flat so we did not account for the influence of topography on the stress field. The geometry of the subduction zone was constructed from the USGS Subduction zone geometry model Slab2 (Hayes et al., 2018), which contours the interface of the subducting Nazca oceanic slab with the overriding South American continental plate, and was limited down to the lithosphere/asthenosphere boundary. On the continental plate, we introduced four crustal-scale faults, with geometries that have been carefully reconstructed from published geological maps and structural cross-sections (Farías et al., 2010; Giambiagi et al., 2012). These are: the San Ramon-Pocuro fault system, El Diablo-Las Le˜nas-El Fierro fault system and the eastern-most thrusts of the Aconcagua-Malargüe foldand- thrust belts and the Frontal Cordillera (see tectonic overview Section 2.1). In the absence of constraints on how these major fault systems interact at depth and in relation to the inter-plate contact, we terminated the faults at a maximum depth of 35 km and drew from published structural cross-sections, which have an underlying assumption of eastvergence, to build their subsurface geometry (Farías et al., 2010b; Giambiagi et al., 2012). We did not explore the published cross sections for a bi-verging orogeny (e.g. Riesner et al., 2018) as the proposed fault interactions are difficult to resolve physically in three dimensions across the entire study area.

To the mesh, we then assigned traction-free boundary conditions to the triangle elements in each dislocation surface, using a uniform crustal Poisson's ratio of 0.25 (Turcotte and Schubert, 2002). Convergence between the South American and Nazca plates was simulated by prescribing slip to the box's east and west walls, which, in turn, deforms the model interior. The current rates of absolute plate motion, relative to hotspots, are 4.8 and 3.2 cm yr□ 1 for the South American and Nazca plates, respectively (Gripp and Gordon, 2002). We therefore assign 60 % of the total opening motion to the continental plate and 40 % to the oceanic plate. The crustal-scale faults were allowed to slip freely but were prohibited from opening motion, while the north and south walls were allowed to slip freely in all directions, to prevent any edge effects.

At the slab interface, we simulated two different regimes. The first, approximated the cumulative effect of subduction seismic events, so simulating the long-term coseismic phase in which the subducting slab is allowed to slip freely in all directions. The second, a long-term interseismic period, where we locked the upper 40 km of the slab interface, approximating the depth of the seismogenic zone at this latitude (Patzwahl et al., 1999).

With these boundary conditions, tribemx uses Green's functions (Meade, 2007) to calculate, firstly, the slip vector, with its corresponding strike and dip slip components, at the centroid of each triangular element (e.g., Aron et al., 2022). Secondly, a displacement vector and its horizontal and vertical components on a regular 10 km grid on the Earth's surface. To assess the dependency of the displacement vector on the resolution of the mesh and assure reproducibility of the numerical model results, we ran the model for a full range of mesh resolutions and calculated the root mean square error of each mesh with respect to the finest (Fig. 3c); a mesh with a characteristic length scale of 8400 m (the approximate size of the triangle's sides). We used the 8400 m grid as the final output and average the results of the seismic and interseismic model runs.

The Green's functions are used to calculate vertical displacement as a percentage of the total convergence rate (e.g., Aron et al., 2022). Using two control points on the Earth's surface we scaled these dimensionless rock uplift values, x:

$$X_{norm} = x - r_{min} / r_{max} - r_{min} (t_{max} - t_{min}) + t_{min}$$

where r_{min} and r_{max} are understood to be the minimum and maximum modelled values of x, and t_{min} and t_{max} are minimum and maximum values of x_{norm}. We find the best fitting t_{min} and t_{max} that can resolve the difference in rock uplift rate between the oceanic slab, where we expect there to be a rock uplift rate of 0 mm/yr, and a site located in the Principle Cordillera, where existing Apatite Fission Track and Apatite Helium age-elevation profiles indicate exhumation rates of 0.3 mm/yr. This scaling yields a t_{max} of 0.41 mm/yr, which is in line with a 0.4 mm/ yr minimum average rock uplift rate approximated at 34°S for the last 5 Ma, from paleo-elevation data (Farías et al., 2008; Hoke et al., 2014; Val et al., 2018). It is also in agreement with minimum slip rates estimated for the San Ramon fault, 0.3 mm/yr over the past 16 Myr, and on its west verging basal detachment, 0.4 mm/yr over the last 25 Myr (Armijo et al., 2010; Vargas et al., 2014). To compare the topographic and rock uplift spatial distributions, we calculated the difference between the datasets once each is normalised by their data range.

4. Results

4.1. River network analysis

Mountain elevation decreases rapidly southwards along both sides of the cordillera, though the highest peaks are in Argentina (Fig. 1c). The highest peaks (>4000 m) are in the north, reaching >5000 m in the Rio Diamante and Rio Atuel Argentinian catchments. In the south, the average peak height is 2000–3000 m, with maximum peak heights of 4000 m in Argentina. The local relief, however, is notably higher in the Chilean cordillera. Here, maximum relief is focused in the north, with >3000 m of local relief in the Rio Cachapoal and Rio Tinguiririca catchments, decreasing to ~1500 m southwards along the Rio Teno and Rio Lontue (Fig. 5c). Higher normalised channel steepness values, >200 ksn (θ=0.37), are also concentrated within the Chilean cordillera, in a band upstream of, but parallel to, the mountain front (Figs. 3 and 4). Channels are uniformly less steep, <100 ksn, in Argentina, where local relief is <2000 m, only reaching higher values around volcanic edifices (Fig. 5c).

An analysis of the full distributions of channel steepness along each river network and the distribution of normalised valley widths reveal further important differences between the Chilean and Argentinian sides of the cordillera (Fig. 6). The Argentinian rivers have median steepness values between 30 and 35. Their median normalised widths are 0.034 and 0.05 along the Rio Malargüe and Rio Atuel, respectively, and 0.003, along the Rio Diamante. The measurements on the latter river were complicated by recent volcanic processes influencing the valley morphology and may therefore be an outlier in this analysis. Conversely, while all Chilean rivers record an upstream steepening (Figs. 4 and 5), their full steepness distributions highlight that Rio Lontue, the southernmost river, is distinct. The Rio Cachapoal, Rio Tinguiririca and Rio Teno have a median steepness of between 40 and 45, while the Rio Lontue has a median steepness of 30, in line with the Argentinian rivers. Their median normalised valley widths, however, are all very similar, ranging between 0.01 and 0.02. The trend of narrow and steeper river networks along the Chilean cordillera is also evident from field investigations (Fig. 2).

4.2. Steepness dependency on bedrock lithology

Rivers draining the Paleozoic basement rocks of the Frontal Cordillera are systematically steeper than those in the Principle Cordillera (Fig. 7). The distributions of channel steepness within the Neogene and Mesozoic bedrocks of the Principle Cordillera, however, are not distinguishable from one another. The lower channel steepness values in the southeast do not therefore appear to be well explained by the differences in bedrock lithology nor age. This finding is corroborated by the uniform channel steepness values recorded across the Mesozoic- Neogene bedrock transition in a number of catchments. Pliocene-Holocene volcanic activity, on the other hand, does appear to have influenced channel steepness patterns locally in the Rio Atuel and to a lesser extent in the Rio Diamante. Along these rivers, low channel steepness distributions in Pliocene-Holocene volcanics (Fig. 7) map onto plateaus of Quaternary volcanic rock (Fig. 1).

4.3. Spatial distribution of rock uplift rates derived from the mechanical model

The variable, vertical rock uplift field generated by our simple mechanical model (Figs. 3d and 5a) is reproducible for the given structural configuration, irrespective of mesh resolution (Fig. 3c). The model also accurately predicts positive rock uplift onshore and zero-net rock uplift along the Pacific coastline (Fig. 3d), and therefore replicates the spatial extent of deformation in the crust (e.g. Cosentino et al., 2018). When averaging the long-term vertical crustal motion over seismic and interseismic periods, we find that deformation is generally focused on the western and eastern fronts of the Principle Cordillera and that the higher magnitude of deformation shifts from the west to the east with increasing latitude (Figs. 3d and 5a). Southwards, rock uplift along the San Ramon-Pocuro fault decreases from 0.4 to 0.3 mm/yr as deformation shifts to the east within the Malargüe fold-and-thrust belt of the Eastern Principle Cordillera.

We therefore predict that rock uplift rates in the Argentinian cordillera are currently highest, within the Malargüe fold-and-thrust belt, where channel steepness and local relief are lowest and valleys are widest. This contrasts with the Chilean cordillera,

where the highest local relief and channel steepness are observed upstream of the high uplift zone along the San Ramon-Pocuro fault (Fig. 5).

5. Discussion

5.1. Tectonic model and topography

Our mechanical modelling predicts a southward shift in the localisation of high rock uplift rates, from the west-verging San Ramon- Pocuro fault to the east-verging Malargüe fold-and-thrust belt (Fig. 3d). There is ample structural and geomorphic evidence to suggest both of these structures have been major active fronts accommodating shortening throughout the Quaternary (Armijo et al., 2010; Branellec et al., 2016; Farías et al., 2008, 2010b; Messager et al., 2010; Riesner et al., 2018; Vargas et al., 2014). In the north of the study area, the preferential accommodation of rock uplift along the west-verging, San Ramon-Pocuro fault, and the passive nature of the El Fierro-El Diablo- Las Lenas fault systems, are in agreement with existing evidence of a biverging orogeny (Armijo et al., 2010; Riesner et al., 2018). The dominance of west-vergent motion during the evolution of the Principle Cordillera can therefore occur without a more complex structural geometry than that previously proposed (c.f. Riesner et al., 2018). To the south, the increasing trend in vertical rock uplift within the Malargüe fold-and-thrust belt is not interpreted from existing estimates of shortening rates in balanced cross-sections (Giambiagi et al., 2012). This disagreement is predictable because our model finds significant oblique motion in this sector of the cordillera, a shortening direction that is not considered when cross-sections are constructed perpendicular to the mountain front.

There are also other processes that can generate vertical motion in the crust that are not related to crustal faulting. Mantle convection in this region favours the maintenance of topography in Argentina (Schellart, 2017), and any isostatic rebound of the crust due to glacial unloading would southwardly increase vertical movement of the crust. These additional processes would therefore support and enhance our model findings of high rock uplift rates in southern Argentina. With this model constraint, we can analyse the extent to which topography and erosional processes record this spatial variability in fault motion. Where our mechanical model predicts a southward increase in tectonic uplift through the study area, we observe a southward decrease in total relief, from >5000 m to <4000 m. Similarly, the lowest local relief and channel steepness indices are found where rock uplift rates are highest, in contrast to what is predicted for bedrock fluvial landscapes, where increased uplift ought to energise streams to incise and steepen (Whipple and Tucker, 1999). Our findings do not therefore support regional tectonic studies that suggest that the topography results from near pure surface homogeneous uplift (Giambiagi et al., 2012). We do, however, note important differences in valley morphology, which suggest other factors must be modulating the morphological response of the landscape to rock uplift.

5.2. Climate and bedrock lithology on topography

As highlighted by previous studies, the broad pattern of decreasing mountain elevation with latitude follows the climate gradient and can be explained either by the southward enhancement of Quaternary glacial erosion (Montgomery et al., 2001) or through the

lubrication of the subduction interface by climate-enhanced sediment delivery to the trench (Lamb and Davis, 2003). Channel steepness, local relief and valley width, on the other hand, which vary over millennial timescales, vary most significantly from west to east. This trend cannot be explained by spatial variability in glacial erosion, firstly, because the main valleys are below the equilibrium line altitude modelled for the last glacial maximum in this region (Clapperton, 1994). Secondly, because models of warm-based glacial erosion would otherwise predict lower gradient valleys in the steeper Chilean cordillera where snowline altitudes are reconstructed at lower elevations (MacGregor et al., 2000).

The obtained values of channel steepness fall below the global threshold identified by Hilley et al. (2019) above which steepness becomes insensitive to erosion rate. Considering that the observed morphological trends are driven primarily by fluvial incision, we explored the drivers of vertical and lateral incision across this landscape. The active western and eastern mountain fronts are bounded by reverse faults. In response to fault slip and earthquakes, we therefore expect efficient rivers to first fill with landslide sediments and then over time, as sediments are evacuated, generate knickpoints proximal to the faults, which then propagate upstream through vertical bedrock incision (Loget and Van Den Driessche, 2009). Upstream reaches distal from the faults, on the other hand, ought to preferentially incise laterally and widen where vertical incision is inhibited by a sediment cover (Yanites et al., 2010). The systematic steepening of rivers and their local relief upstream of the San Ramon-Pocuro fault has been well-explained by such a detachment-limited model for a propagating erosional wave (Farías et al., 2008). Valley widening upstream and downstream of the active knickpoint zones, together with their vast sediment stores, suggests sediment cover has modulated river incision to some extent in these Chilean rivers. The strong overlap in the distributions of channel steepness and bedrock valley width for each catchment (Fig. 3) suggest their response to rock uplift has been relatively uniform, irrespective of their lithological differences.

This trend is in stark contrast to those rivers draining the Argentinian cordillera. Here, the river valleys are wider and less steep along their lengths, despite their predicted high rates of fault-induced vertical motion (Fig. 5a). The broad groupings of bedrock lithology mapped hinder us from investigating the role of local variability in erodibility; e.g. internal discontinuities from cooling or structural pre-conditioning on valley geometry. Indeed, local lithological constraints on valley geometry are evident, particularly around volcanic centres that have been active over the last 2 million years. Our analysis of channel steepness distributions within the broad bedrock units (Fig. 7), however, allows us to observe that the broad differences in bedrock age and lithology are not the dominant control on cordillera-scale differences in river morphology. These morphological differences do, however, map onto hemispheric-scale precipitation patterns that have mostly likely persisted for the last 14 Ma (Viale et al., 2019).

5.3. Conceptual model for the south Central Andes

A river's ability to evacuate its sediment supply and respond sensitively to fault vertical movement can be limited if its transport capacity is low. In wet mountain ranges such

as the Himalayas, sediment evacuation can occur over years to decades (Whipp and Ehlers, 2019). In arid mountain ranges, such as the south Central Andes, however, effective discharge, or the frequency of effective discharge events, can become an important factor limiting the erosional response time to rock uplift. In Fig. 8, we suggest that the wetter, Chilean rivers have responded to fault uplift on the San Ramon-Pocuro fault by generating a propagating knick zone proximal to the fault, and widening river valleys upstream, distal from the fault, as conceptualised by Yanites et al. (2010). In contrast, the drier Argentinian rivers have responded more slowly to fault motion along the Malargüe and Aconcagua fold-and-thrust belts. They have not yet been able to incise vertically due to the delayed evacuation of their sediment covers, thereby promoting lateral incision and valley widening along their lengths (Fig. 6).

Farías et al. (2008) previously estimated a delayed erosion response time to rapid uplift in the Chilean Cordillera of 5–10 Ma, calculated from evidence of knick-point propagation through volcanic rocks of known emplacement ages. The lack of bedrock exposure and steepening in the Argentinian Principle cordillera suggests even longer response times, much >10 Ma. This has resulted in very different fluvial landscapes developing on either side of the drainage divide (Fig. 2).

5.4. Wider implications

With this work, we highlight the process through which long-term climate has modulated bedrock valley morphology, and therefore fluvial erosion, in response to rock uplift of the Andean Principle Cordillera. These findings go some way to supporting the hypothesis that latitudinal variations in millennial and decadal erosion rates in the Chilean Andes record spatial variability in the erosional response time of the Andes to Miocene uplift, modulated by climate (Carretier et al., 2015). They also highlight that caution should be taken when using river networks to invert information about tectonic activity in arid landscapes. Without independent constraint on the spatial distribution of fault motion across the Argentinian cordillera, relatively high rock uplift rates would have been overlooked in this region and would not have been interpreted by classical river profile inversion techniques (e.g. Goren et al., 2014; Aron et al., 2022).

5.5. Future sensitivity to climate change

Models suggest that landscapes should most sensitively respond to changes in the mean annual precipitation rate between 100 mm/yr and 1500 mm/yr (DiBiase and Whipple, 2011). As this is the range of precipitation rates in our study area, differences in valley morphology and sediment cover on either side of the Principle Cordillera's drainage divide offer an opportunity to identify thresholds for climate influencing morphological change. The Argentinian cordillera currently has a mean annual precipitation rate of <500 mm/yr and a variability in average monthly discharge of 170 % (Araneo and Villalba, 2014). Here, the lack of erosional response to faulting suggests the rivers are tending towards being transport-limited. Their low mean annual rainfall and infrequency of high magnitude rainfall events may be important in limiting not only their sensitivity to a tectonically-induced slope, but also maintaining slopes that have a high threshold for sediment mobility, through time. This transport-limited behaviour is a precondition that may impact the future sensitivity of this landscape to

climatic change. The migration rate of such rivers across wide sediment filled valleys can be a geomorphic filter that buffers the link between the frequency and magnitude of rainfall events, and erosion and sediment export in these catchments. The impact of such internal feedbacks within the sediment system on sediment transfer is well documented in alluvial rivers downstream of mountain fronts (Harries et al., 2019).

The more detachment-limited style of river profile evolution evident in the Chilean rivers occurs where there is currently a minimum average rainfall of 800 mm/yr, a strong orographic rainfall gradient, and only a 50 % variance in average monthly discharge (Fig. 1). The steeper and narrower valleys of the Chilean rivers (Fig. 2) have evolved through sediment filling and evacuation and have generated large (~40 m) terraces through this process (Fig. 2). This suggests sediment has been mobilized through these wetter catchments in the past and that any increases in the frequency of large mobilising events could have a direct impact on the delivery of sediment downstream into highly populated areas. Future research into how a landscape's initial and boundary conditions influence its response to climatic change is necessary to understand the hazard posed by geomorphic change in these regions.

6. Conclusion

Here we provided an example of climate modulating the contrasting morphological response of both sides of the south Central Andean topography to tectonic uplift. Using a mechanical model to predict the spatial distribution of rock uplift across the cordillera, produced by subduction and displacement along crustal faults, we are able to observe where the morphology of the Andes has responded to rock uplift and which factors may be otherwise modulating the tectonic-topographic link. In response to tectonic rock uplift, we observe large differences between the steepness, local relief and valley widths of the Chilean and Argentinian cordilleras. Rock uplift along the San Ramon-Pocuro fault in the Chilean Andes is correlated with an upstream zone of steep river channels, high local relief and narrow valleys. In contrast, the zone of most rapid rock uplift in southeast Argentina, along the Malargüe foldand- thrust belt, has not caused rivers to steepen but instead to widen and fill with sediment. Given the correlation between these morphological trends and long-term climate patterns, we suggest climate aridity in Argentina has limited the ability of these catchments to evacuate their sediment supply and incise vertically, instead promoting lateral incision and valley widening. We recognise climate patterns that persist over millennial timescales as being an important limiting factor in delaying a river's morphological response to rock uplift. This finding has important implications for understanding the erosional sensitivity of landscapes to both tectonic and climatic forcing.

Declaration of competing interest

The authors declare that they have no known competing financial interests or personal relationships that could have appeared to influence the work reported in this paper.

Data availability

Data will be made available on request.

Acknowledgements

The authors are grateful for the support of the ANID Fondo Nacional de Desarrollo Científico y Tecnol´ogico (FONDECYT-Chile) Postdoctoral Project no. 3201048, and Fondo de Financiamiento de Centros de Investigacion en Areas Prioritarias (Chile) Project ANID/FONDAP/ 15110017 2022 (CIGIDEN). We would like to thank Anne Mather and two anonymous reviewers as well as Editor Martin Stokes for their helpful feedback that strengthened the manuscript. The triangular mesh of the Andean subduction zone is available at https://github.com/rebekaharries/MeshAndes.git.

References

Adams, B.A., Whipple, K.X., Forte, A.M., Heinmsath, A.M., Hodges, K.V., 2020. Climate controls on erosion in tectonically active landscapes. Sci. Adv. 6 https://doi.org/ 10.1126/sciadv.aaz3166.

Araneo, D., Villalba, R., 2014. Variability in the annual cycle of the Río Atuel streamflows and its relationship with tropospheric circulation. Int. J. Climatol. 35, 2948–2967. https://doi.org/10.1002/joc.4185.

Armijo, R., Rauld, R., Thiele, R., Vargas, G., Campos, J., Lacassin, R., Kausel, E., 2010. The West Andean Thrust, the San Ram´on Fault, and the seismic hazard for Santiago, Chile. Tectonics 29 (2), TC2007. https://doi.org/10.1029/2008tc002427.

Aron, F., Johnstone, S.A., Mavrommatis, A.P., Sare, R.M., Maerten, F., Loveless, J.P., Baden, C.W., Hilley, G.E., 2022. Mountain rivers reveal the earthquake hazard of geologic faults in Silicon Valley. Geophys. Res. Lett. 49, 19, e2022GL099220 https:// doi.org/10.1029/2022GL099220.

Arriagada, C., Ferrando, R., C´ordova, L., Morata, D., Roperch, P., 2013. The Maipo orocline: a first scale structural feature in the miocene to recent geodynamic evolution in the Central Chilean Andes. Andean Geol. https://doi.org/10.5027/ andgeoV40n3-a02.

Arrospide, F., Mao, L., Escauriaza, C., 2018. Morphological evolution of the Maipo River in central Chile: Influence of instream gravel mining. Geomorphology 306, 182–197. https://doi.org/10.1016/j.geomorph.2018.01.019.

Barnhart, K.R., Tucker, G.E., Doty, S.G., Shobe, C.M., Glade, R.C., Rossi, M.W., Hill, M.C., 2020. Inverting Topography for Landscape Evolution Model Process Representation: 2. Calibration and Validation. J. Geophys. Res. Earth Surf. 125 https://doi.org/ 10.1029/2018JF004963.

Baynes, E.R.C., Lague, D., Steer, P., Bonnet, S., Illien, L., 2020. Sediment Flux-Driven Channel Geometry Adjustment of Bedrock and Mixed Gravel–Bedrock Rivers. Process. Landf, Earth Surf. https://doi.org/10.1002/esp.4996.

Branellec, M., Nivi`ere, B., Callot, J.P., Regard, V., Ringenbach, J.C., 2016. Evidence of Active Shortening Along the Eastern Border of the San Rafael Basement Block: Characterization of the Seismic Source of the Villa Atuel Earthquake (1929). Geol. Mag, Mendoza province, Argentina. https://doi.org/10.1017/S0016756816000194.

Brocard, G.Y., van der Beek, P.A., 2006. Influence of incision rate, rock strength, and bedload supply on bedrock river gradients and valley-flat widths: Field-based evidence and calibrations from western Alpine rivers (southeast France), in: Tectonics, Climate, and Landscape Evolution. Geological Society of America. https://doi.org/10.1130/2006.2398(07.

Carretier, S., Tolorza, V., Rodríguez, M.P., Pepin, E., Aguilar, G., Regard, V., Martinod, J., Riquelme, R., Bonnet, S., Brichau, S., H´erail, G., Pinto, L., Farías, M., Charrier, R., Guyot, J.L., 2015. Erosion in the Chilean Andes between 27◦S and 39◦S: tectonic, climatic and geomorphic control. Geol. Soc. Lond. Spec. Publ. https://doi.org/10.1144/sp399.16.

Carretier, S., Tolorza, V., Regard, V., Aguilar, G., Bermúdez, M.A., Martinod, J., Guyot, J. L., H´erail, G., Riquelme, R., 2018. Review of erosion dynamics along the major N-S climatic gradient in Chile and perspectives. Geomorphology. https://doi.org/10.1016/j.geomorph.2017.10.016.

Clapperton, C., 1994. The quaternary glaciation of Chile: a review. Rev. Chil. Hist. Nat. 67, 369–383.

Cook, K.L., Turowski, J.M., Hovius, N., 2014. River gorge eradication by downstream sweep erosion. Nat. Geosci. 7, 682–686. https://doi.org/10.1038/ngeo2224.

Cosentino, N.J., Aron, F., Crempien, J.G.F., Jordan, T.E., 2018. Role of subducted sediments in plate interface dynamics as constrained by Andean forearc (paleo) topography, in: Ingersoll, R.V., Lawton, T.F., Graham, S.A. (Eds.), Tectonics, Sedimentary Basins, and Provenance: A Celebration of the Career of William R. Dickinson, Geological Society of America Special Publication 540, 43–63. https://doi.org/10.1130/2018.2540(03).

Dadson, S.J., Hovius, N., Chen, H., Dade, W.B., Lin, J.-C., Hsu, M.-L., Lin, C.-W., Horng, M.-J., Chen, T.-C., Milliman, J., Stark, C.P., 2004. Earthquake-triggered increase in sediment delivery from an active mountain belt. Geology 32 (8), 733–736. https://doi.org/10.1130/G20639.1.

Desormeaux, C., Godard, V., Lague, D., Duclaux, G., Fleury, J., Benedetti, L., Bellier, O., 2022. and the ASTER Team: Investigation of stochastic-threshold incision models across a climatic and morphological gradient. Earth Surf. Dynam. 10, 473–492. https://doi.org/10.5194/esurf-10-473-2022.

DiBiase, R.A., Whipple, K.X., 2011. The influence of erosion thresholds and runoff variability on the relationships among topography, climate, and erosion rate. J. Geophys. Res. Earth Surf. https://doi.org/10.1029/2011JF002095.

Dosseto, A., Hesse, P.P., Maher, K., Fryirs, K., Turner, S., 2010. Climatic and vegetation control on sediment dynamics during the last glacial cycle. Geology 38, 395–398. https://doi.org/10.1130/G30708.1.

England, P., Molnar, P., 1990. Surface uplift, uplift of rocks, and exhumation of rocks. Geology 18 (12), 1173–1177. https://doi.org/10.1130/0091-7613(1990)018<1173:SUUORA>2.3.CO;2.

Evenstar, L.A., Hartley, A.J., Mather, A.E., 2023. Orogenic-orographic feedback and the rise of the Central Andes. Earth & Planet. Sci. Lett. 602, 117931 https://doi.org/10.1016/j.epsl.2022.117931.

Farías, M., Charrier, R., Carretier, S., Martinod, J., Fock, A., Campbell, D., C´aceres, J.,Comte, D., 2008. Late Miocene high and rapid surface uplift and its erosional response in the Andes of central Chile (33◦–35◦S): Uplift and erosion in central Chile Andes. Tectonics 27. https://doi.org/10.1029/2006TC002046.

Farías, M., Comte, D., Charrier, R., Martinod, J., David, C., Tassara, A., Tapia, F., Fock, A., 2010. Crustal-scale structural architecture in central Chile based on seismicity and surface geology: Implications for Andean mountain building. Tectonics 29 (3), TC3006. https://doi.org/10.1029/2009TC002480.

Ferrier, K., Huppert, K., Perron, J., 2013. Climatic control of bedrock river incision. Nature 496, 206–209. https://doi.org/10.1038/nature11982.

Gasparini, N.M., Brandon, M.T., 2011. A generalized power law approximation for fluvial incision of bedrock channels. J. Geophys. Res. Earth Surf. https://doi.org/10.1029/2009JF001655.

Geuzaine, C., Remacle, J.-F., 2009. Gmsh: a 3-D finite element mesh generator with builtin pre- and post-processing facilities. Int. J. Numer. Methods Eng. 79, 1309–1331.https://doi.org/10.1002/nme.2579.

Giambiagi, L.B., Ramos, V.A., Godoy, E., Alvarez, P.P., Orts, S., 2003. Cenozoic deformation and tectonic style of the Andes, between 33° and 34° south latitude. Tectonics 22 (4). https://doi.org/10.1029/2001TC001354.

Giambiagi, L., Mescua, J., Bechis, F., Tassara, A., Hoke, G., 2012. Thrust belts of the southern Central Andes: Along-strike variations in shortening, topography, crustal geometry, and denudation. Bull. Geol. Soc. Am. https://doi.org/10.1130/B30609.1.

Goren, L., Fox, M., Willett, S.D., 2014. Tectonics from Fluvial Topography Using Formal Linear Inversion: Theory and Applications to the Inyo Mountains. J. Geophys. Res. F Earth Surf, California. https://doi.org/10.1002/2014JF003079.

Gripp, A.E., Gordon, R.G., 2002. Young tracks of hotspots and current plate velocities. Geophys. J. Int. 150, 321–361. https://doi.org/10.1046/j.1365-246X.2002.01627.x.

Harries, R.M., Kirstein, L.A., Whittaker, A.C., Attal, M., Main, I., 2019. Impact of recycling and lateral sediment input on grain size fining trends—Implications for reconstructing tectonic and climate forcings in ancient sedimentary systems. Basin Res. 31, 866–891. https://doi.org/10.1111/bre.12349.

Harries, R.M., Kirstein, L.A., Whittaker, A.C., Attal, M., Peralta, S., Brookes, S., 2018. Evidence for self-similar bedload transport on Andean alluvial fans, Iglesia Basin, South Central Argentina. J. Geophys. Res. Earth Surf. 123, 9. https://doi.org/ 10.1029/2017JF004501.

Harries, R.M., Gailleton, B., Kirstein, L.A., Attal, M., Whittaker, A.C., Mudd, S.M., 2021.

Impact of climate on landscape form, sediment transfer and the sedimentary record. Earth Surf. Process. Landf. 46, 990–1006. https://doi.org/10.1002/esp.5075.

Harrison, S., Mighall, T., Stainforth, D.A., Allen, P., Macklin, M., Anderson, E., Knight, J., Mauquoy, D., Passmore, D., Rea, B., Spagnolo, M., Shannon, S., 2019. Uncertainty in geomorphological responses to climate change. Clim. Chang. 156, 69–86. https://doi.org/10.1007/s10584-019-02520-8.

Hayes, G.P., Moore, G.L., Portner, D.E., Hearne, M., Flamme, H., Furtney, M., Smoczyk, G.M., 2018. Slab2, a comprehensive subduction zone geometry model. Science 362 (6410), 58–61. https://doi.org/10.1126/science.aat4723.

Hilley, G.E., Porder, S., Aron, F., Baden, C.W., Johnstone, S.A., Liu, F., Sare, R.M., Steelquist, A., Young, H.H., 2019. Earth's topographic relief potentially limited by an upper bound on channel steepness. Nat. Geosci. https://doi.org/10.1038/s41561-019-0442-3.

Hobley, D.E.J., Sinclair, H.D., Mudd, S.M., Cowie, P.A., 2011. Field calibration of sediment flux dependent river incision. J. Geophys. Res. Earth Surf. 116 https://doi.org/10.1029/2010JF001935.

Hoggard, M., Austermann, J., Randel, C., Stephenson, S., 2021. Observational estimates of dynamic topography through space and time. In: Ballmer, M., Cottaar, S., Konter, J. (Eds.), Marquardt, H. Wiley, Geophysical Monograph Series, pp. 371–411.https://doi.org/10.1002/9781119528609.ch15.

Hoke, G.D., Giambiagi, L.B., Garzione, C.N., Mahoney, J.B., Strecker, M.R., 2014. Neogene paleoelevation of intermontane basins in a narrow, compressional mountain range, southern Central Andes of Argentina. Earth Planet. Sci. Lett. https://doi.org/10.1016/j.epsl.2014.08.032.

Jeffery, M.L., Yanites, B.J., Poulsen, C.J., Ehlers, T.A., 2014. Vegetation-precipitation controls on Central Andean topography. J. Geophys. Res. Earth Surf. 119, 1354–1375. https://doi.org/10.1002/2013JF002919.

Kay, Suzanne, Mpodozis, Constantino, 2002. Magmatism as a probe of Neogene shallowing of the Nazca Plate beneath the modern Chilean flat-slab. J. S. Am. Earth Sci. 15, 39–57. https://doi.org/10.1016/S0895-9811(02)00005-6.

Kirby, E., Whipple, K., 2001. Quantifying differential rock-uplift rates via stream profile analysis. Geology. https://doi.org/10.1130/0091-7613(2001)029<0415:QDRURV>2.0.CO;2.

Kirby, E., Whipple, K.X., 2012. Expression of active tectonics in erosional landscapes. J. Struct. Geol. https://doi.org/10.1016/j.jsg.2012.07.009.

Lague, D., 2010. Reduction of long-term bedrock incision efficiency by short-term alluvial cover intermittency: Bedrock incision and alluvial cover intermittency. J. Geophys. Res. Earth Surf. 115 https://doi.org/10.1029/2008JF001210.

Lai, L.S.H., Roering, J.J., Finnegan, N.J., Dorsey, R.J., Yen, J.Y., 2021. Coarse sediment supply sets the slope of bedrock channels in rapidly uplifting terrain: Field

and topographic evidence from eastern Taiwan. Earth Surf. Process. Landf. 46 (13), 2671–2689. https://doi.org/10.1002/esp.5200.

Lamb, S., Davis, P., 2003. Cenozoic climate change as a possible cause for the rise of the Andes. Nature 425, 792–797. https://doi.org/10.1038/nature02049.

Leonard, J.S., Whipple, K.X., 2021. Influence of Spatial Rainfall Gradients on River Longitudinal Profiles and the Topographic Expression of Spatially and Temporally Variable Climates in Mountain Landscapes. J. Geophys. Res. Earth Surf. 126 https://doi.org/10.1029/2021JF006183.

Li, T., Fuller, T.K., Sklar, L.S., Gran, K.B., Venditti, J.G., 2020. A Mechanistic Model for Lateral Erosion of Bedrock Channel Banks by Bedload Particle Impacts. J. Geophys.Res. Earth Surf. 125 https://doi.org/10.1029/2019JF005509.

Litvak, V.D., Poma, S., Jones, R.E., Paz, L.F., Iannelli, S.B., Spagnuolo, M., Kirstein, L.A., Folguera, A., Ramos, V.A., 2018. The Late Paleogene to Neogene Volcanic Arc in the Southern Central Andes (28◦–37◦ S). In: The Evolution of the Chilean-Argentinean Andes. Springer Earth System Sciences. Springer, Cham. https://doi.org/10.1007/978-3-319-67774-3_20.

Loget, N., Van Den Driessche, J., 2009. Wave train model for knickpoint migration. Geomorphology 106, 376–382. https://doi.org/10.1016/j.geomorph.2008.10.017.

Loveless, J.P., 2019. tribem: Boundary element code using triangular dislocation elements. doi:https://doi.org/10.5281/zenodo.3333899.

MacGregor, K.R., Anderson, R.S., Anderson, S.P., Waddington, E.D., 2000. Numerical simulations of glacial-valley longitudinal profile evolution. Geology. https://doi.org/10.1130/0091-7613(2000)028<1031:NSOGVL>2.3.CO;2.

Marshall, S.T., Cooke, M.L., Owen, S.E., 2009. Interseismic deformation associated with three-dimensional faults in the greater Los Angeles region. California. J. Geophys. Res. Solid Earth 114. https://doi.org/10.1029/2009JB006439.

Masiokas, M.H., Rabatel, A., Rivera, A., Ruiz, L., Pitte, P., Ceballos, J.L., Barcaza, G.,Soruco, A., Bown, F., Berthier, E., Dussaillant, I., MacDonell, S., 2020. A review of the current state and recent changes of the Andean cryosphere. Front. Earth Sci. 8 https://doi.org/10.3389/feart.2020.00099.

McQuarrie, N., 2002. The kinematic history of the central Andean fold-thrust belt, Bolivia: Implications for building a high plateau. Geol. Soc. Am. Bull. 114, 950–963.https://doi.org/10.1130/0016-7606(2002)114<0950:TKHOTC>2.0.CO;2.

McQuarrie, N., DeCelles, P., 2001. Geometry and structural evolution of the central Andean backthrust belt, Bolivia. Tectonics 20 (5), 669–692. https://doi.org/10.1029/2000TC001232.

Meade, B.J., 2007. Algorithms for the calculation of exact displacements, strains, and stresses for triangular dislocation elements in a uniform elastic half space. Comput.Geosci. https://doi.org/10.1016/j.cageo.2006.12.003.

Melnick, D., Echtler, H.P., 2006. Inversion of forearc basins in south-central Chile caused by rapid glacial age trench fill. Geology 34 (9), 709–712. https://doi.org/10.1130/G22440.1.

Mescua, J.F., Giambiagi, L.B., Tassara, A., Gimenez, M., Ramos, V.A., 2014. Influence of pre-Andean history over Cenozoic foreland deformation: Structural styles in the Malargüe fold-and-thrust belt at 35°S, Andes of Argentina. Geosphere 10, 585–609.https://doi.org/10.1130/GES00939.1.

Messager, G., Niviere, B., Martinod, J., Lacan, P., Xavier, J.P., 2010. Geomorphic Evidence for Plio-Quaternary Compression in the Andean Foothills of the Southern Neuqun Basin. Tectonics, Argentina. https://doi.org/10.1029/2009TC002609.

Montgomery, D.R., Balco, G., Willett, S.D., 2001. Climate, tectonics, and the morphology of the Andes. Geology. https://doi.org/10.1130/0091-7613(2001)029<0579:CTATMO>2.0.CO;2.

Müller, J.P., Kley, J., Jacobshagen, V., 2002. Structure and Cenozoic kinematics of the Eastern Cordillera, southern Bolivia (21◦S). Tectonics 21 (5), 1037. https://doi.org/10.1029/2001TC001340.

Patzwahl, R., Mechie, J., Schulze, A., Giese, P., 1999. Two-dimensional velocity models of the Nazca Plate subduction zone between 19.5◦S and 25◦S from wide-angle seismic measurements during the CINCA95 project. J. Geophys. Res. Solid Earth 104,7293–7317. https://doi.org/10.1029/1999JB900008.

Pearson, D., Kapp, P., DeCelles, P.G., Reiners, P., Gehrels, G., Ducea, M., Pullen, A., 2013. Influence of pre-Andean crustal structure on Cenozoic thrust belt kinematics and shortening magnitude: Northwestern Argentina. Geosphere 9, 1–17. https://doi.org/10.1130/GES00923.1.

Perron, J.T., 2017. Climate and the Pace of Erosional Landscape Evolution. Annu. Rev. Earth Planet. Sci. 45, 561–591. https://doi.org/10.1146/annurev-earth-060614-105405.

Perron, J.T., Royden, L., 2013. An integral approach to bedrock river profile analysis. Earth Surf. Process. Landf. 38 (6), 570–576. https://doi.org/10.1002/esp.3302.

Poveda, G., Espinoza, J.C., Zuluaga, M.D., Solman, S.A., Garreaud, R., van Oevelen, P.J., 2020. High Impact Weather Events in the Andes. Earth Sci, Front. https://doi.org/10.3389/feart.2020.00162.

Racano, S., Schildgen, T.F., Cosentino, D., Miller, S.R., 2021. Temporal and spatial variations in rock uplift from river-profile inversions at the central Anatolian Plateau southern margin. J. Geophys. Res. Earth Surf. 126 https://doi.org/10.1029/2020JF006027.

Rehak, K., Bookhagen, B., Strecker, M.R., Echtler, H.P., 2010. The Topographic Imprint of a Transient Climate Episode: The Western Andean Flank between 15·5° and 41·5°S. Process. Landf, Earth Surf. https://doi.org/10.1002/esp.1992.

Riebe, C.S., Sklar, L.S., Lukens, C.E., Shuster, D.L., 2015. Climate and topography control the size and flux of sediment produced on steep mountain slopes. Proc. Natl. Acad. Sci. https://doi.org/10.1073/pnas.1503567112.

Riesner, M., Lacassin, R., Simoes, M., Armijo, R., Rauld, R., Vargas, G., 2017. Kinematics of the active West Andean fold-and-thrust belt (central Chile): Structure and longterm shortening rate. Tectonics 36, 287–303. https://doi.org/10.1002/2016TC004269.

Riesner, M., Lacassin, R., Simoes, M., Carrizo, D., Armijo, R., 2018. Revisiting the crustal structure and kinematics of the central Andes at 33.5◦S: implications for the mechanics of Andean mountain building. Tectonics. https://doi.org/10.1002/2017TC004513.

Schellart, W.P., 2017. Andean mountain building and magmatic arc migration driven by subduction-induced whole mantle flow. Nat. Commun. 8 https://doi.org/10.1038/s41467-017-01847-z.

Schwanghart, W., Scherler, D., 2014. Short communication: TopoToolbox 2 – MATLAB based software for topographic analysis and modeling in Earth surface sciences. Earth Surf. Dyn. 2, 1–7. https://doi.org/10.5194/esurf-2-1-2014.

Schwanghart, W., Ryan, M., Korup, O., 2018. Topographic and seismic constraints on the vulnerability of Himalayan hydropower. Geophys. Res. Lett. 45, 17. https://doi.org/10.1029/2018GL079173.

Seagren, E.G., Schoenbohm, L.M., Owen, L.A., Figueiredo, P.M., Hammer, S.J., Rimando, J.M., Wang, Y., Bohon, W., 2020. Lithology, topography, and spatial variability of vegetation moderate fluvial erosion in the south-central Andes. Earth & Planet. Sci. Lett. 551 https://doi.org/10.1016/j.epsl.2020.116555.

Shobe, C.M., Turowski, J.M., Nativ, R., Glade, R.C., Bennett, G.L., Dini, B., 2021. The role of infrequently mobile boulders in modulating landscape evolution and geomorphic hazards. Earth-Sci. Rev. 220, 103717 https://doi.org/10.1016/j.earscirev.2021.103717.

Silvestro, J., Kraemer, P., Achilli, F., Brinkworth, W., 2005. Evolucion de las cuencas sinorogenicas de la cordillera principal entre 35◦ y 36◦S, Malargüe. Rev. Asoc. Geol. Argent. 60, 627–643.

Sklar, L.S., Dietrich, W.E., 2004. A mechanistic model for river incision into bedrock by saltating bed load. Water Resour. Res. https://doi.org/10.1029/2003WR002496.

Sklar, L.S., Dietrich, W.E., 2006. The role of sediment in controlling steady-state bedrock channel slope: Implications of the saltation–abrasion incision model. Geomorphology 82, 58–83. https://doi.org/10.1016/j.geomorph.2005.08.019.

Stalder, N.F., Herman, F., Fellin, M.G., Coutand, I., Aguilar, G., Reiners, P.W., Fox, M., 2020. The Relationships between Tectonics, Climate and Exhumation in the Central Andes (18–36°S): Evidence from Low-Temperature Thermochronology. Rev, Earth- Sci. https://doi.org/10.1016/j.earscirev.2020.103276.

Tolorza, V., Mohr, C.H., Carretier, S., Serey, A., Sepúlveda, S.A., Tapia, J., Pinto, L., 2019. Suspended sediments in Chilean rivers reveal low postseismic erosion after the Maule earthquake (Mw 8.8) during a severe drought. J. Geophys. Res. Earth Surf. 124 https://doi.org/10.1029/2018JF004766.

Turcotte, D.Lawson, Schubert, Gerald, 2002. Geodynamics, 2nd Edition. ed. Cambridge University Press, Cambridge; New York.

Val, P., Venerdini, A.L., Ouimet, W., Alvarado, P., Hoke, G.D., 2018. Tectonic control of erosion in the southern Central Andes. Earth Planet. Sci. Lett. https://doi.org/10.1016/j.epsl.2017.11.004.

Vargas, G., Klinger, Y., Rockwell, T.K., Forman, S.L., Rebolledo, S., Baize, S., Lacassin, R., Armijo, R., 2014. Probing large intraplate earthquakes at the west flank of the Andes. Geology 42, 1083–1086. https://doi.org/10.1130/G35741.1.

Viale, M., Bianchi, E., Cara, L., Ruiz, L.E., Villalba, R., Pitte, P., Masiokas, M., Rivera, J., Zalazar, L., 2019. Contrasting Climates at both Sides of the Andes in Argentina and Chile. Environ. Sci, Front. https://doi.org/10.3389/fenvs.2019.00069.

Wapenhans, I., Fernandes, V.M., O'Malley, C., White, N., Roberts, G.G., 2021. Scale dependent contributors to river profile geometry. J. Geophys. Res. Earth Surf. 126 https://doi.org/10.1029/2020JF005879.

Whipp, D.M., Ehlers, T.A., 2019. Quantifying Landslide Frequency and Sediment Residence Time in the Nepal Himalaya. Adv, Sci. https://doi.org/10.1126/sciadv. aav3482.

Whipple, K.X., 2002. Implications of sediment-flux-dependent river incision models for landscape evolution. J. Geophys. Res. https://doi.org/10.1029/2000jb000044.

Whipple, K.X., Tucker, G.E., 1999. Dynamics of the stream-power river incision model: implications for height limits of mountain ranges, landscape response timescales, and research needs. J. Geophys. Res. Solid Earth 104. https://doi.org/10.1029/ 1999JB900120.

Wickert, A.D., Schildgen, T.F., 2019. Long-profile evolution of transport-limited gravelbed rivers. Earth Surf. Dyn. 7, 17–43. https://doi.org/10.5194/esurf-7-17-2019.

Yanites, B.J., 2018. The dynamics of channel slope, width, and sediment in actively eroding bedrock river systems. J. Geophys. Res. Earth Surf. 123, 1504–1527. https:// doi.org/10.1029/2017JF004405.

Yanites, B.J., Tucker, G.E., Mueller, K.J., Chen, Y.-G., 2010. How rivers react to large earthquakes: evidence from central Taiwan. Geology 38, 639–642. https://doi.org/ 10.1130/G30883.1.

Yanites, B.J., Tucker, G.E., Hsu, H.-L., Chen, C., Chen, Y.-G., Mueller, K.J., 2011. The influence of sediment cover variability on long-term river incision rates: an example from the Peikang River, central Taiwan. J. Geophys. Res. 116, F03016. https://doi. org/10.1029/2010JF001933.

Figure captions

Fig. 1. a) Geology, b) climate and c) topography of the Andean cordillera. The four crustal-scale structures accommodating shortening in response to plate convergence are delineated along with the location of the Chilean trench and coastline. Map a) demonstrates the difference in bedrock age and lithology between the Chilean (Cenozoic sedimentary-volcaniclastics) and Argentinian (Mesozoic sedimentary-volcaniclastics) cordillera. Map b) highlights the strong and persistent rain shadow gradient from west to east across the cordillera, mapped using worldclim data on mean annual rainfall. Map c) shows the southward reduction in mountain elevation. The black square delineates the focus area for our river analysis.

Fig. 2. Field photos (a and b) and google earth images (c and d) of two rivers in Chile and Argentina, respectively. The Rio Teno, in Chile, has a relatively narrow valley with terrace sequences (up to 40 m high) along its sides and steep, high local relief. The Rio Atuel, in Argentina, has a wide valley with a meandering, sinuous river channel and low local relief.

Fig. 3. a) Plan view of the 3D mesh used to model fault slip in response to plate convergence. b) Cross-section looking north highlighting the fault geometries reconstructed from existing literature. c) Root mean square error calculated with respect to the finest resolution mesh, demonstrating the lack of dependency of the rock uplift field on the characteristic element length. d) Uplifted field predicted by the tectonic model when averaged over seismic (locked) and aseismic (unlocked) slip modes. Control points 1 and 2 were used to scale the non-dimensional field to realistic values. We focused our topographic analysis within the black box.

Fig. 4. Chi-Elevation long profiles for each river flowing perpendicular to the mountain front.

Fig. 5. Spatial variability in (a) modelled rock uplift rate, (b) normalised channel steepness and (c) local relief. The spatial differences between (d) normalised channel steepness and modelled rock uplift and (e) local relief and modelled rock uplift.

Fig. 6. Distribution of normalised main valley width plotted against the normalised channel steepness distribution of the drainage network for each river. The error bars are the 25th and 75th percentiles of each distribution. Purple rivers drain the western Chilean cordillera and green rivers drain the eastern, Argentinian cordillera.

Fig. 7. Distributions of channel steepness within the different geomaterials mapped in Fig. 1a.

Fig. 8. Conceptual model of how Chilean and Argentinian rivers have responded to fault motion, adapted from Yanites et al. (2010). On both sides of the cordillera, rock uplift decays upstream from frontal thrusts. Following landslide filling of the river valleys, the wetter Chilean rivers evacuated enough of their sediment supply in their proximal zone to propagate knickzone upstream from the fault. In contrast, the lower transport capacity of the arid Argentinian rivers has limited the evacuation of their sediment cover and inhibited vertical incision, promoting lateral incision and widening of their valleys along their lengths.

Figure 1.

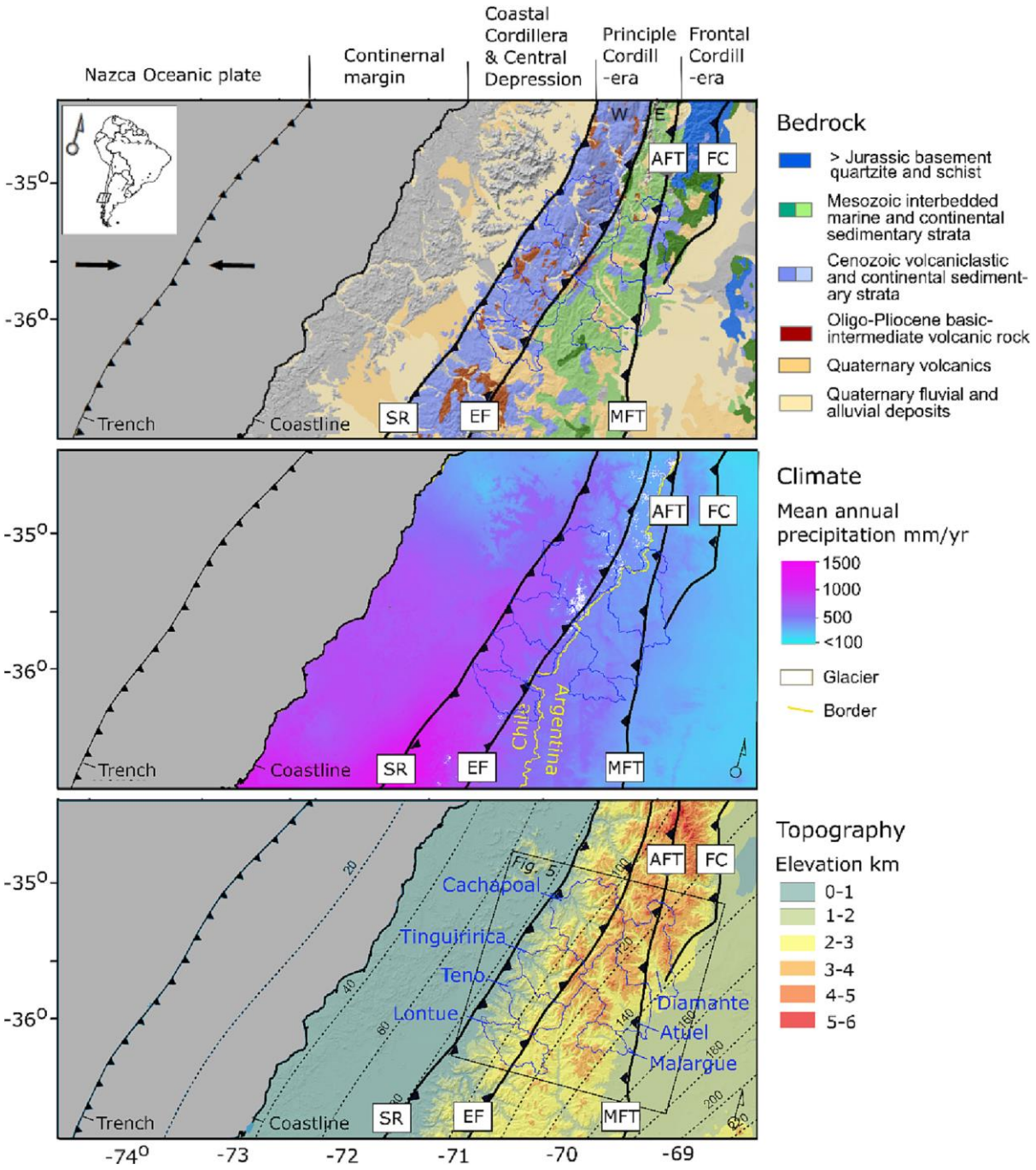
Nazca Oceanic plate
Continernal margin
Coastal Cordillera & Central Depression
Principle Cordill -era
Frontal Cordill -era
W
E
AFT
FC
SR
EF
MFT
Trench
Coastline
-35°
-36°
Bedrock
> Jurassic basement quartzite and schist
Mesozoic interbedded marine and continental sedimentary strata
Cenozoic volcaniclastic and continental sedimentary strata
Oligo-Pliocene basic-intermediate volcanic rock
Quaternary volcanics
Quaternary fluvial and alluvial deposits
Climate
Mean annual precipitation mm/yr
1500
1000
500
<100
Glacier
Border
Argentina
Chile
Topography
Elevation km
0-1
1-2
2-3
3-4
4-5
5-6
Fig. 5
Cachapoal
Tinguiririca
Teno
Lontue
Diamante
Atuel
Malargüe
-74°
-73
-72
-71
-70
-69

Figure 2.

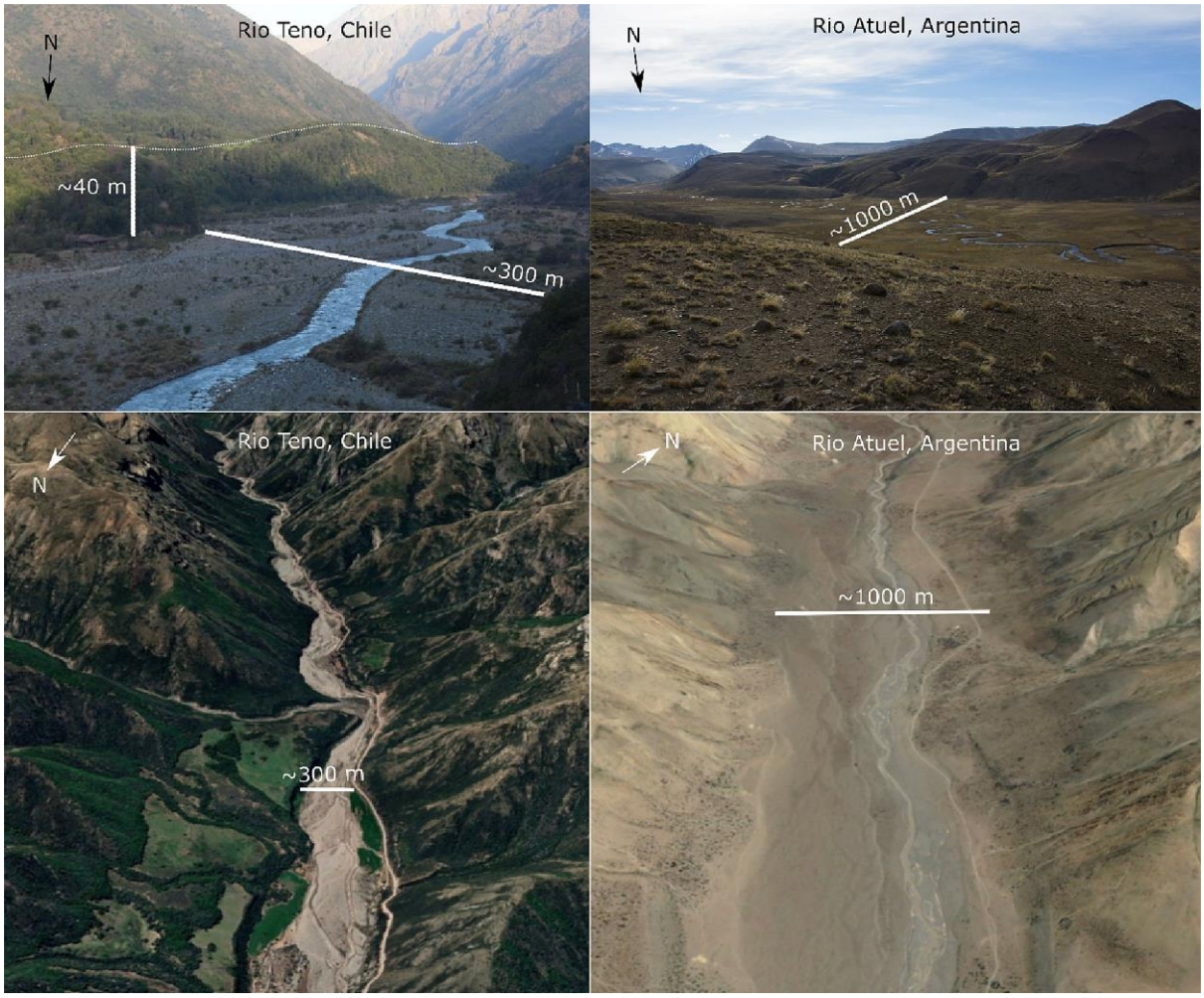
Rio Teno, Chile
N
~40 m
~300 m
Rio Atuel, Argentina
N
~1000 m
Rio Teno, Chile
N
~300 m
Rio Atuel, Argentina
N
~1000 m

Figure 3.

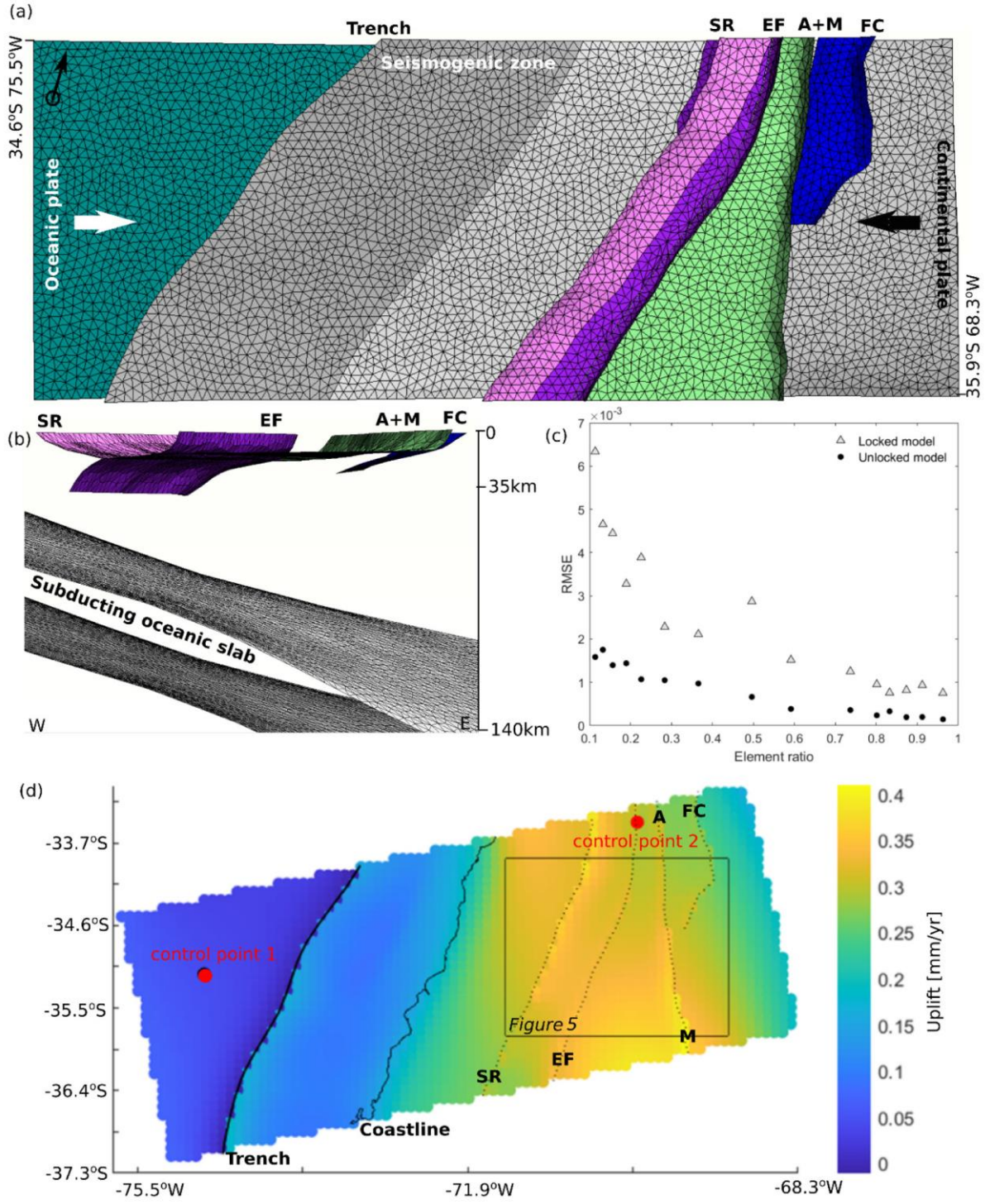
(a)
Trench
SR
EF
A+M
FC
34.6°S 75.5°W
Seismogenic zone
Oceanic plate
Continental plate
35.9°S 68.3°W
(b)
SR
EF
A+M
FC
0
35km
140km
Subducting oceanic slab
W
E
(c)
×10^-3
Locked model
Unlocked model
RMSE
Element ratio
(d)
-33.7°S
-34.6°S
-35.5°S
-36.4°S
-37.3°S
-75.5°W
-71.9°W
-68.3°W
A
FC
control point 2
control point 1
Figure 5
M
EF
SR
Coastline
Trench
Uplift [mm/yr]

Figure 4.

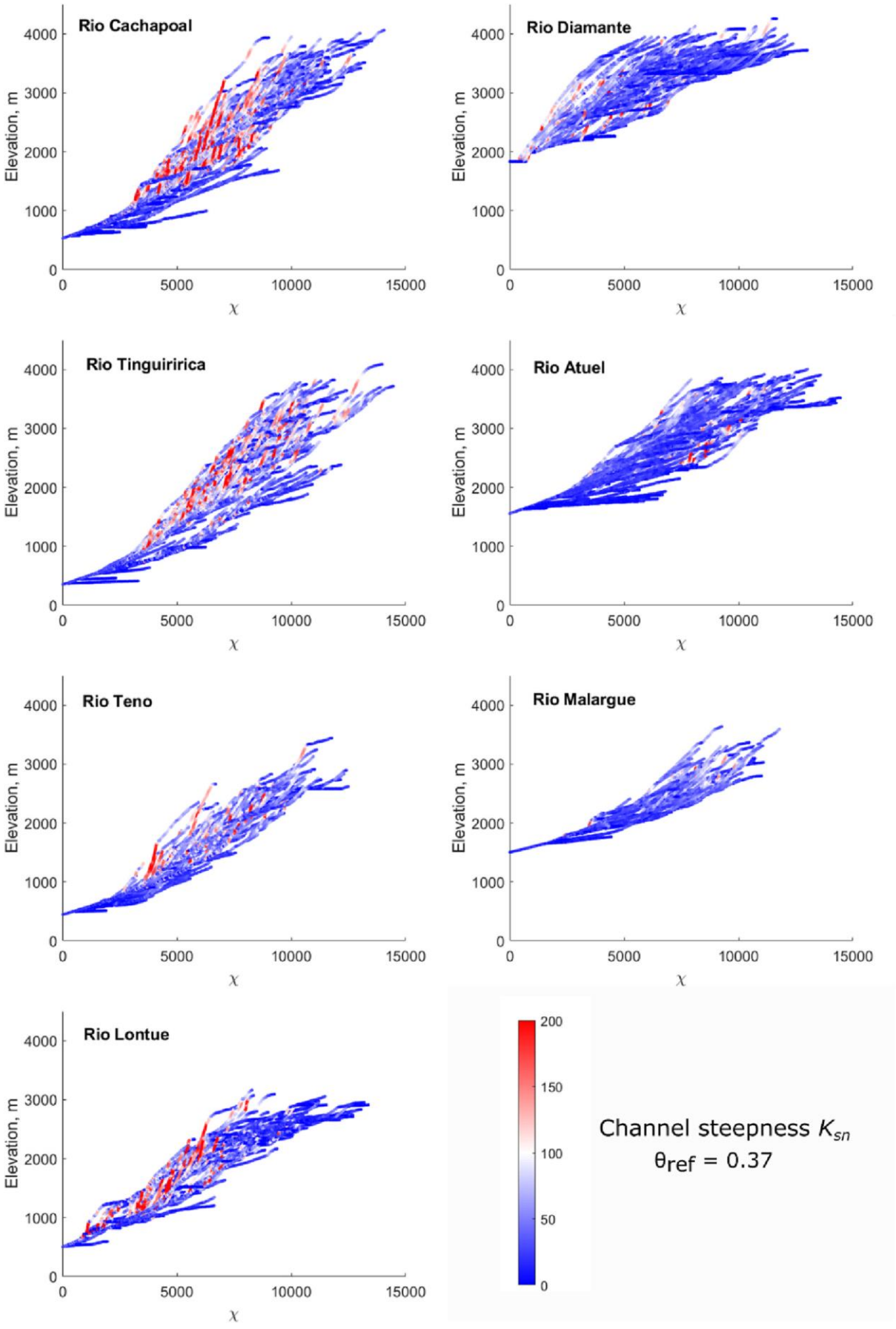
Rio Cachapoal
Rio Diamante
Rio Tinguiririca
Rio Atuel
Rio Teno
Rio Malargue
Rio Lontue
Elevation, m
χ
0
1000
2000
3000
4000
5000
10000
15000
200
150
100
50
Channel steepness K_{sn}
θ_{ref} = 0.37

Figure 5.

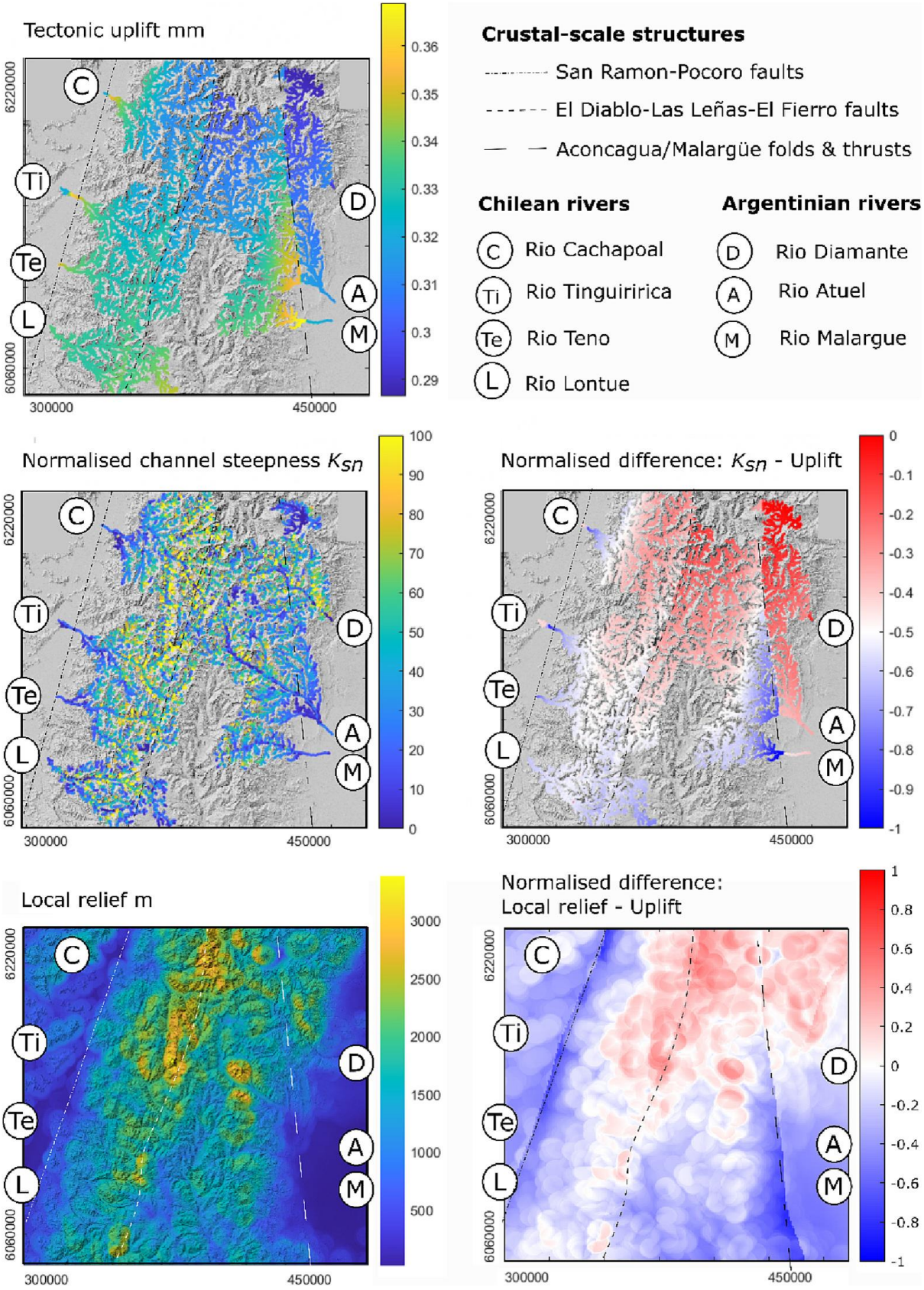
Tectonic uplift mm
0.36
0.35
0.34
0.33
0.32
0.31
0.3
0.29
Crustal-scale structures
San Ramon-Pocoro faults
El Diablo-Las Leñas-El Fierro faults
Aconcagua/Malargüe folds & thrusts
Chilean rivers
C Rio Cachapoal
Ti Rio Tinguiririca
Te Rio Teno
L Rio Lontue
Argentinian rivers
D Rio Diamante
A Rio Atuel
M Rio Malargue
Normalised channel steepness K_{sn}
100
90
80
70
60
50
40
30
20
10
0
Normalised difference: K_{sn} - Uplift
0
-0.1
-0.2
-0.3
-0.4
-0.5
-0.6
-0.7
-0.8
-0.9
-1
Local relief m
3000
2500
2000
1500
1000
500
Normalised difference:
Local relief - Uplift
1
0.8
0.6
0.4
0.2
0
-0.2
-0.4
-0.6
-0.8
-1
6220000
6060000
300000
450000

Figure 6.

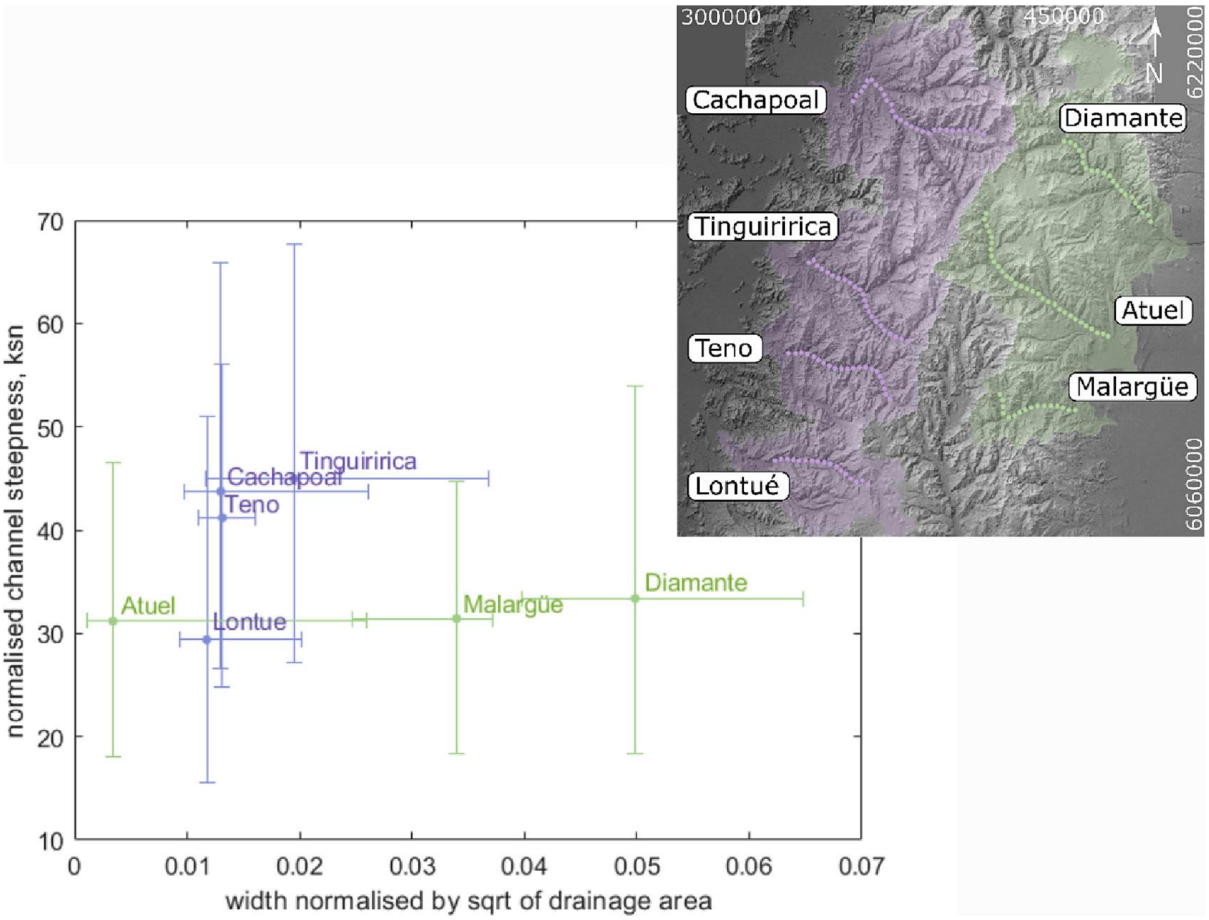
300000
450000
6220000
6060000
N
Cachapoal
Diamante
Tinguiririca
Atuel
Teno
Malargüe
Lontué
normalised channel steepness, ksn
width normalised by sqrt of drainage area
Tinguiririca
Cachapoal
Teno
Atuel
Lontue
Malargüe
Diamante
70
60
50
40
30
20
10
0
0.01
0.02
0.03
0.04
0.05
0.06
0.07

Figure 7.

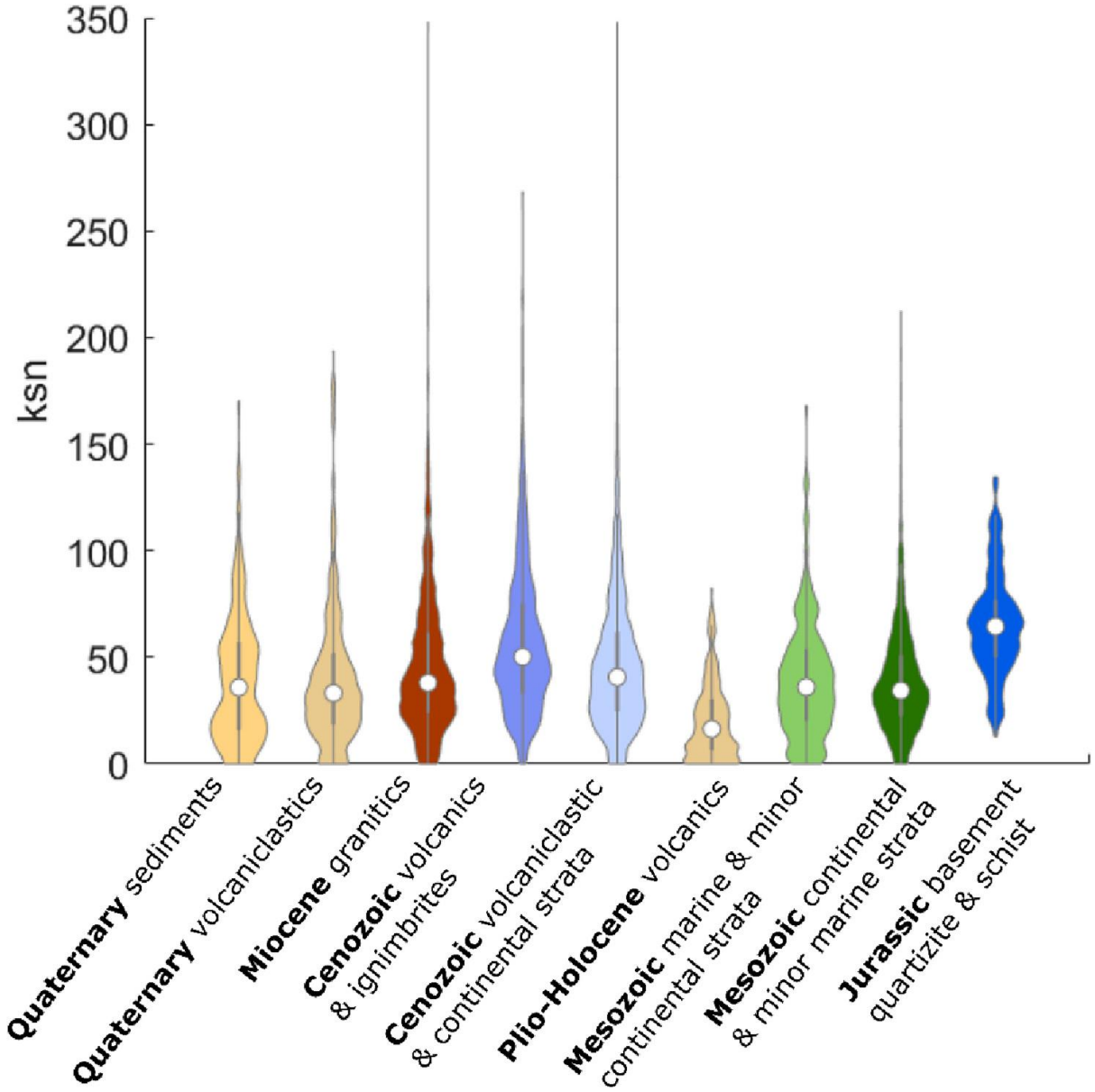
ksn
350
300
250
200
150
100
50
0
Quaternary sediments
Quaternary volcaniclastics
Miocene granitics
Cenozoic volcanics & ignimbrites
Cenozoic volcaniclastic & continental strata
Plio-Holocene volcanics
Mesozoic marine & minor continental strata
Mesozoic continental & minor marine strata
Jurassic basement quartizite & schist

Figure 8.